Available online at www.sciencedirect.com
SCIENCE DIRECT®
Estuarine, Coastal and Shelf Science 56 (2003) 629–639
ESTUARINE COASTAL AND SHELF SCIENCE

Tidal truncation and barotropic convergence in a channel network tidally driven from opposing entrances

J.C. Warner[a,b,*], D. Schoellhamer[a], G. Schladow[b]

[a]U.S. Geological Survey, Sacramento, CA, USA
[b]University of California, Davis, CA, USA

Received 16 October 2001; received in revised form 4 March 2002; accepted 19 March 2002

Abstract

Residual circulation patterns in a channel network that is tidally driven from entrances on opposite sides are controlled by the temporal phasing and spatial asymmetry of the two forcing tides. The Napa/Sonoma Marsh Complex in San Francisco Bay, CA, is such a system. A sill on the west entrance to the system prevents a complete tidal range at spring tides that results in tidal truncation of water levels. Tidal truncation does not occur on the east side but asymmetries develop due to friction and off-channel wetland storage. The east and west asymmetric tides meet in the middle to produce a barotropic convergence zone that controls the transport of water and sediment. During spring tides, tidally averaged water-surface elevations are higher on the truncated west side. This creates tidally averaged fluxes of water and sediment to the east. During neap tides, the water levels are not truncated and the propagation speed of the tides controls residual circulation, creating a tidally averaged flux in the opposite direction.

Keywords: channel network; tidal truncation; residual circulation; barotropic convergence; San Francisco Bay

1. Introduction

Estuarial and coastal settings may consist of complex geometric patterns that create channels subjected to tidal forcings from both ends. Circulation patterns of water and suspended sediment through these systems are controlled by the magnitude and phasing of the bounding tidal forcings. Previous analytical investigations on canals subjected to tidal forcings at both ends have concentrated on solutions to linearized governing equations. Einstein and Fuchs (1954) and Parsons (1918) used similar sets of equations to describe the currents and water-level variations in the Cape Cod Canal and the proposed Panama Sea Level Canal, respectively. Dronkers (1964, p. 240) derived a more general expression with dependence on the total flow with the solution then applicable to any channel shape. Wong (1990) developed a linearized, frequency-dependent model to examine spatial distributions of tidal and subtidal variability along the length of the Chesapeake and Delaware Canal. All of these investigations considered deep channels with small ratios of tidal amplitude to mean water depth ($\eta/h \ll 1$). Resulting water levels were functions of the phase and magnitude of the driving water levels at the ends of the canal and the velocities essentially were determined by a balance between friction and the elevation head difference between the ends of the canal (Wilcox, 1958). The time of current reversal may not coincide directly with the time of head reversal, owing to the need to overcome the momentum of the system.

In a more shallow system, Parker (1991) briefly demonstrated the effect of a dominant semidiurnal water level, but a quarter-diurnal current variation due to a linear superposition of opposing (cancelling) predominant M2 currents that allowed M4 terms to become dominant and additive.

The shallow water tidal slough channels for the present study area (ratio of tidal displacement (η) to

* Corresponding author.
E-mail address: jcwarner@usgs.gov (J.C. Warner).

0272-7714/03/$ - see front matter © 2003 Elsevier Science B.V. All rights reserved.
doi:10.1016/S0272-7714(02)00213-5

mean depth is in the order of 1) are shown in Fig. 1. The tidal forcing is a shallow water gravity wave that originates from the Pacific Ocean and enters San Francisco Bay through the Golden Gate, propagating through Central Bay to enter the study area from two directions: (1) northward across the broad shallow San Pablo Bay and into the west entrance at Sonoma Creek, and (2) eastward along the main shipping channel to Carquinez Strait and into the east entrance at the Napa River. Between these two entrances, the study area consists of a network of interconnected tidal channels with depths in the order of 2 m (relative to mean lower low water (MLLW)) and a tidal range of 2 m. The Napa River has a depth of 9 m MLLW near the mouth and decreases to approximately 4 m MLLW near the upper part of the study area (Warner, Schladow, and Schoellhamer, 1999).

The purpose of this paper is to describe the physical processes that control the tidal and tidally averaged time scale circulation patterns in a shallow channel network that is tidally driven from opposing entrances. These physical processes result in temporal and spatial asymmetry in the channel system.

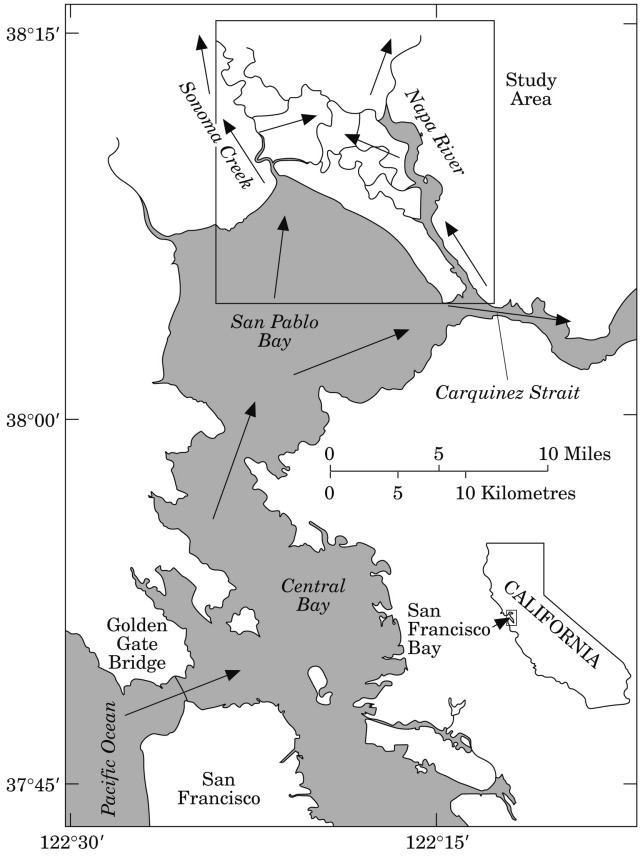

Fig. 1. General flood current directions in study area, San Francisco Bay, CA.

2. Data collection

Equipments to measure water conductivity, temperature and depth (CTD), and velocity magnitude and direction using acoustic Doppler profilers (ADP) or electromagnetic current metres (EMCM) (Table 1) were deployed at eight sites (Fig. 2): Pablo, Socr, SNS, Hude, Buchli, Pipe, MIC, and M5 from 2 September 1997 to 12 March 1998. Additionally, water-level data are referenced from the long-term US Geological Survey (USGS) station, PSP. Measurements at all sites typically were recorded on a 10-min time step. Continuous data sets were not obtained from all the sites for all parameters due to instrument difficulties and biological fouling (Warner et al., 1999).

2.1. Tidal truncation effects

Tidal truncation occurs when the water level does not experience a complete tidal range. This can occur on the landward side of a sill where the water level only reduces to the level of the sill at low tide. On the seaward side of the sill, the water level can reduce to match the forcing ocean tide. To explain this process and its effects in the study area, harmonic analysis is first used to describe the propagation of the tide, then principal components analysis (PCA) denotes the spatial extent of the truncation influence, and, lastly, a momentum balance shows the effects of tidal truncation.

2.1.1. Water-level harmonic analysis

To determine spatial development of tidal asymmetries and to quantify the propagation of the tide from both ends of the system, the measured water-level time series for all sites were first decomposed into their harmonic constants using a least-squares analysis computer program developed by Foreman (1978) and modified by Gartner (1997) for a USGS standard data format. The data used for the analysis typically consisted of the continuous first 3 months of recoverable water-level record from each site, during which time freshwater inflow was constant and minimal. Freshwater inflows have

Table 1
Heights of instruments above the bed

	Vertical distance (m) from the bed to the sensor	
Site	CTD	Velocity
M5	1, 6	ADP—0.5 m bins
MIC	1, 7	ADP—0.5 m bins
Buchli, SNS, Hude, Pipe	0.3	EMCM—0.45 m
Socr, Pablo	0.3	EMCM—0.45 m

m: Metres; CTD: conductivity, temperature, depth; ADP: acoustic Doppler profiler; EMCM: electromagnetic current metre.

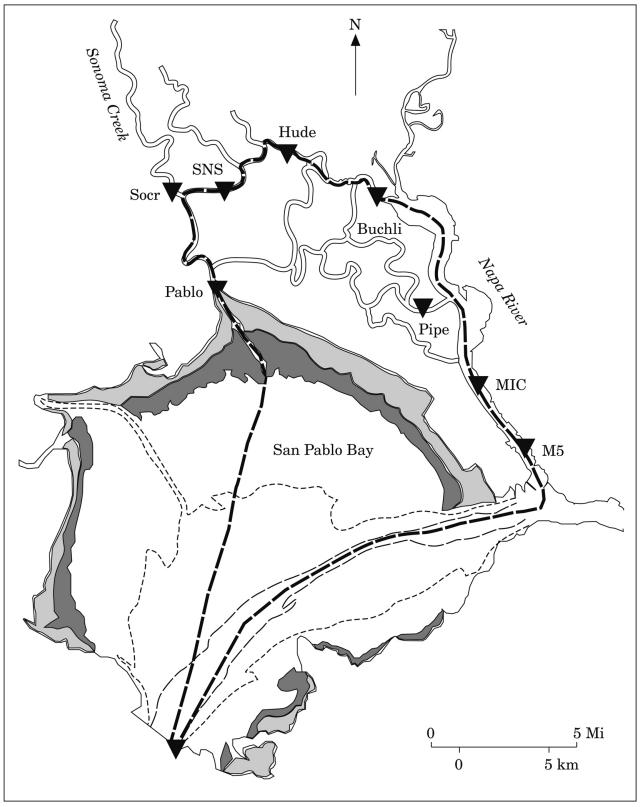

Fig. 2. Loop of sites PSP–Pablo–Socr–SNS–Hude–Buchli–MIC–M5. Bathymetry of San Pablo Bay obtained from Jaffe, Smith, and Zink (1998) (http://sfbay.wr.usgs.gov/access/sanpablobay/bathy/bathy.html). ▫, marsh; ▪, tidal mudflat; – – – –, 6-foot contour mean lower low water; — — —, 30-foot contour mean lower low water; ▬ ▬ ▬, loop of sites; ▼, data collection site.

been shown to alter the phase and amplitude of tidal constituents (Parker, 1991) and therefore this period of low flow was selected. All of the sites showed dominate astronomical constituents of M2, K1, and O1, as typically is observed in San Francisco Bay (Walters, Cheng, & Conomos, 1985). The principal harmonic constituents resolved at each site are given in Table 2. Error analysis on the residual signal (original series less the harmonic components) revealed maximum errors in amplitude and phase in the order of 1 cm and 6°, respectively.

The M2 constituent is the most dominant partial tide (based on its amplitude) and its phase can be used to characterize the propagation of the tide throughout the system. As one enters the slough system from either side the M2 arrival time becomes progressively later towards the middle. Fig. 3 shows the arrival time of the tide at each site based on the M2 constituent of water level. An estimate of the propagation speed of the tide is $c = \sqrt{gh}$ and using average depths of 3 m for the west side (Sonoma Creek) and 7 m for the east side (Napa River) yield speeds of 5.5 and 8.5 m s^{-1}, respectively. The distance from Pablo to SNS is 6500 m which gives a travel time of approximately 6500 m/(5.5 m s^{-1})= 20 min. Fig. 3 shows the arrival of the M2 partial tide as 17 min, which is comparable. Travel times on the east side are faster because of the greater depths and the 16,400 m distance is travelled by the M2 partial tide in 33 min from site M5 to Buchli. Fig. 3 also shows that the incoming tide arrives first at the west side in the order of 5 min.

Because the largest astronomical tidal constituents are the M2, O1, and K1, the resulting predominant shallow water tides will be the M4, MO3, and MK3, of which the last two components enhance diurnal inequality (Aubrey & Speer, 1985). The M4 is responsible for creating temporal asymmetry such as a longer duration to low tide. Increased amplitudes of these shallow water constituents identify locations of increased tidal asymmetry. The magnitudes of these shallow water constituents (Fig. 4) are plotted spatially along the loop of sites PSP–Pablo–Socr–SNS–Hude–Buchli–MIC–M5 (Fig. 2). Amplification of shallow water tides occurs near and on the landward side of site Pablo. However, as one travels along the navigable path past Hude and to the east side of the network, the magnitudes of the shallow water partial tides decrease. For example, the MO3 has a magnitude of 6.5 cm at site Pablo, but it decreases to less than one-half of this (3 cm) at site PSP. The decrease suggests that some physical process near site Pablo is producing nonlinearities in the tide.

Table 2
Selected water-level tidal harmonic constituents

	Diurnal		Semidiurnal		Compound		Overtide
Site	23.93 h, K1	26.87 h, O1	12.42 h, M2	12.00 h, S2	8.39 h, MO3	8.18 h, MK3	6.21 h, M4
Pablo	32.1/132.0	19.5/127.2	64.3/22.4	13.6/27.1	6.4/87.9	5.6/70.3	4.3/329.8
Socr	32.2/140.7	18.5/134.6	66.1/34.5	13.3/44.1	6.7/93.3	4.7/68.1	3.4/329.9
SNS	32.1/138.9	18.3/132.6	66.4/30.81	13.4/41.0	6.8/88.1	4.6/63.4	3.4/325.6
Hude	31.8/144.3	18.2/135.7	71.2/39.8	14.7/51.2	5.6/113.5	2.5/93.7	1.2/286.6
Buchli[a]	32.2/140.8	–	69.1/40.9	–	–	–	2.4/255.8
MIC	25.1/124.0	20.0/123.2	65.4/27.1	16.5/22.0	3.5/107.0	1.7/110.6	1.1/268.1
M5	26.8/122.9	19.5/124.2	61.6/25.0	15.2/18.6	3.5/101.8	1.5/86.8	1.9/248.7
PSP	35.3/120.0	21.5/110.2	59.4/3.7	13.2/3.25	2.9/106.7	2.2/135.8	1.6/73.5

Constituent values shown as amplitude/degrees. Amplitude is given in centimetres and phase is given in degrees. – Implies unresolved constituents.

[a] Short time series due to instrument difficulties.

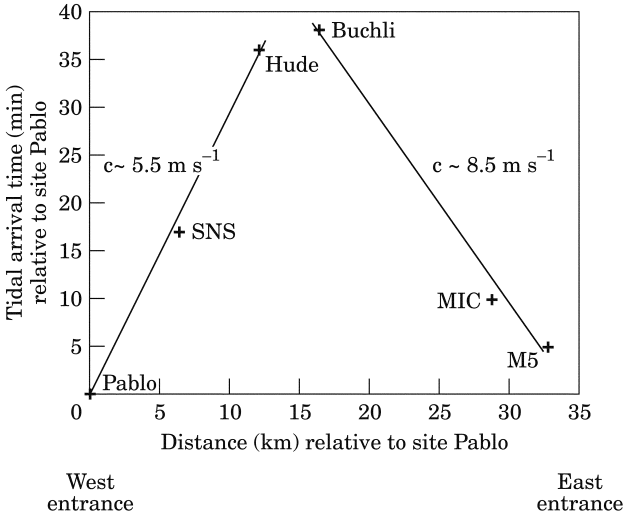

Fig. 3. Arrival time of tide (based on phase of M2 constituent of water level) relative to site Pablo vs. distance from site Pablo. Slopes provide approximate propagation speed of the tide (c) and show a faster travel time on the east side.

A water-level prediction was performed using the same harmonic constants (principal and nonlinear constituents) and for the same time period as for the water-level analysis (Fig. 5). The predicted time series for site M5 compares favourably with the original measured time series, however, the predicted time series of water level for site Pablo does not fit well, especially when depths slowly decrease to the lower low tides. This nonreproducibility of the tide from harmonic constants is an indication of the occurrence of a nonlinear, nonharmonic physical process. This process has been observed by Lincoln and Fitzgerald (1988) and is termed tidal truncation.

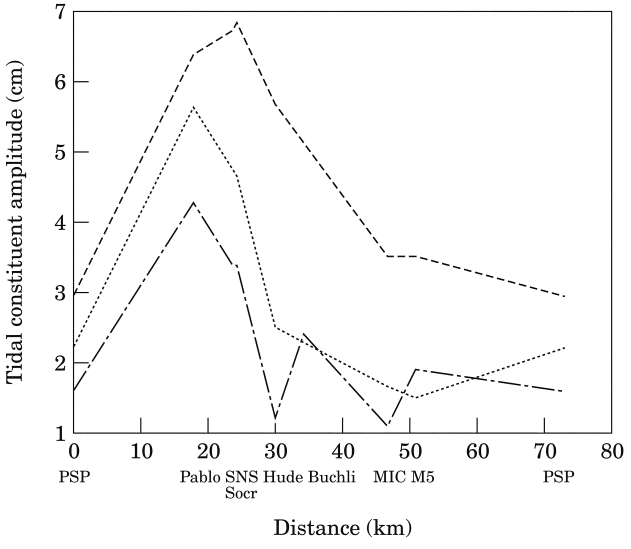

Fig. 4. Spatial variation of selected shallow water tidal harmonic constituents from analysis of water level for loop PSP–Pablo–Socr–SNS–Hude–Buchli–MIC–M5. Maximum tidal nonlinearities occur near site Pablo (- - -, MO3; ·····, MK3; —·—·—, M4).

Tidal truncation occurs when an obstruction to the flow is present in the main channel, truncating the tide for the low water levels. A low-lying tidal mudflat cuts across the entrance to Sonoma Creek (Fig. 2) with depths less than 0 ft below MLLW. This mudflat acts as a sill or an obstruction to the flow. On the landward side of the sill, the tidal water-level fluctuations are truncated at the level of the sill, whereas on the seaward side of the sill, the water level can descend to match the forcing tide. Site Pablo is located on the landward side of the sill and, therefore, will display the truncating effect. Thus, a full ebb from Sonoma Creek (past site Socr, Pablo, and the west side) will not be allowed to develop, and the start to the rising tide will also be delayed.

Tidal truncation effects are greatest during spring tides when the tidal range is increased, as observed by comparing the water-level time series from sites Pablo and M5. During spring tides (Fig. 6a), the increased tidal range allows the water level at site M5 (and in the bay) to decrease below the level of the sill. At these times, an increased frictional effect and the sill elevation prevent the flow at site Pablo from ebbing completely. The slow decrease of water level observed at site Pablo most likely is due to a steady discharge from Sonoma Creek and associated drainage from tidal wetlands in the system. Therefore, the time to 'low tide' will continue until the rising tide has had the opportunity to overtop the sill elevation. The low tide occurs 1.5 h after low tide at site M5 for the lower low tide (Fig. 6a). This spring tide had a slight diurnal inequality, and the higher low tide has a 0.5-h lag behind the low tide on the east side. In either case, this delay will be shown to be critical for circulation patterns in the network. During neap tides (Fig. 6b) the timing of low tide almost is in phase with, or occurs earlier at, site Pablo than at site M5. The difference occurs because the elevation of the low tides does not fall below the sill elevation in San Pablo Bay, and the ebb on the west side is not truncated.

2.1.2. Water-level principal components analysis

To determine the spatial extent of the truncation effect, PCA was performed on the water-level time series. PCA (Preisendorfer, 1988) is a numerical method that represents n time series as n components (eigenvectors) that co-vary in time (Fig. 7). The relative contribution of each component is determined by the eigenvalues of the covariance matrix of the time series. For the analysis of the water-level time series, the first three principal components contain 98% of the variability of the system and explain 95, 2, and 1% of the variance, respectively.

Fig. 7 shows the spatial variation of each principal component and their associated amplitude time series. PC1 is spatially homogenous and the amplitude time series corresponds to the astronomical tidal variability

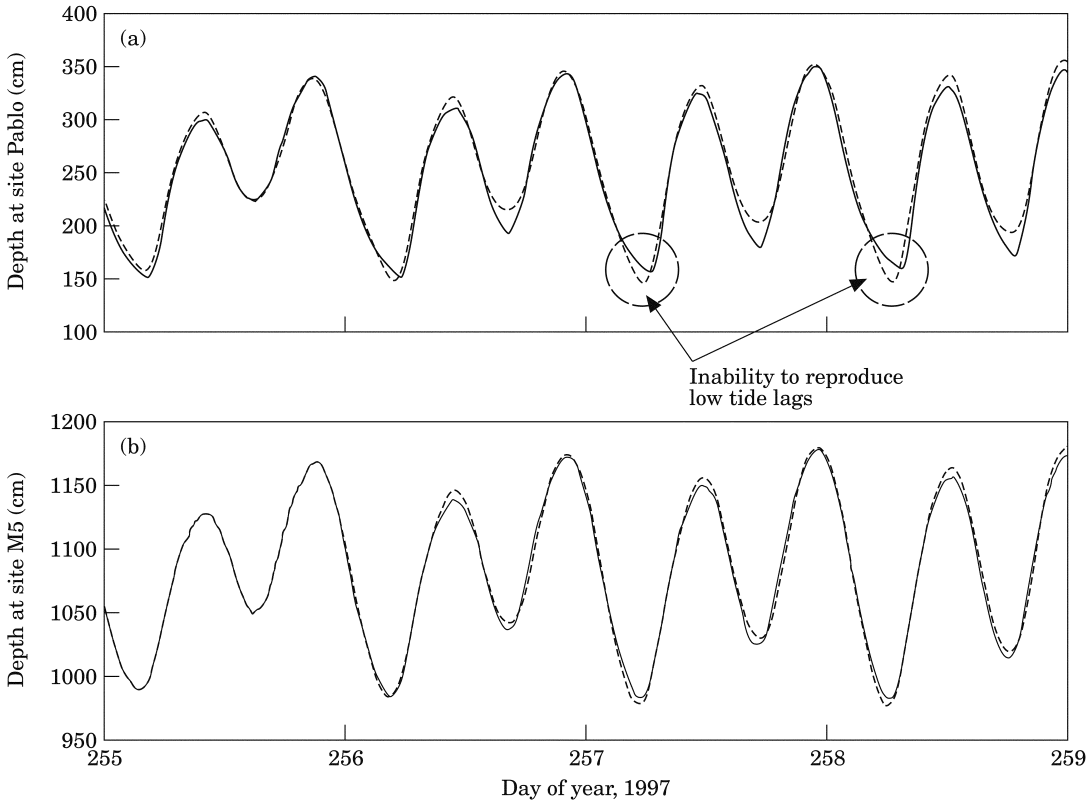

Fig. 5. Comparison of measured and harmonically predicted time series of water level from sites (a) Pablo and (b) M5. The reconstruction of the time series for site Pablo cannot reproduce the long lags at low water (—, field data; - - - -, reconstructed).

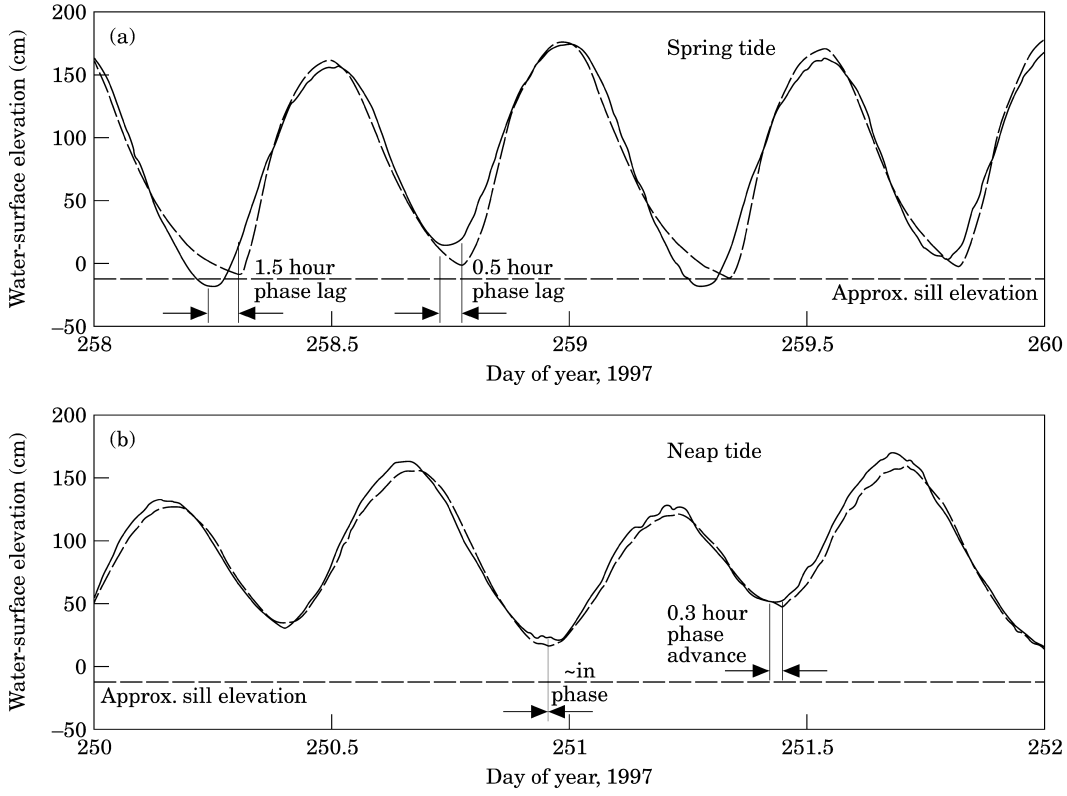

Fig. 6. Influence of tidal sill truncation. (a) Spring tides showing increased tidal asymmetry at site Pablo, especially at lower low water, (b) neap tides showing negligible shallow water truncation. Note: M5 water level approximated, Pablo water level related to survey datum of WGS-84 (—, M5; ———, Pablo).

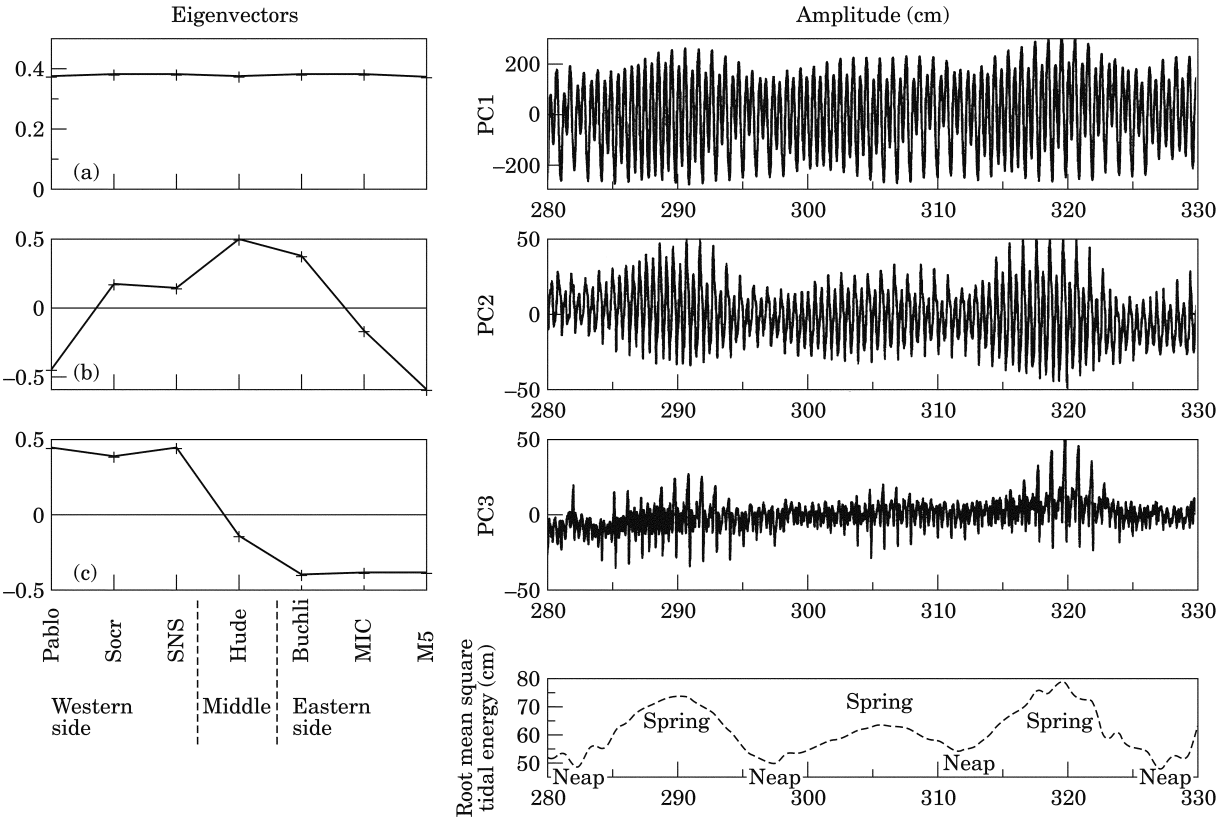

Fig. 7. Principal components and associated amplitude time series for water-level analysis. Eigenvectors show the magnitude of each component at each site. The time series show how each component varies in time. PC3 is used to demarcate the study area into three regions.

of the system, representing the semidiurnal and spring/neap tidal variability. PC2 varies spatially from negative values at the two boundary stations to a positive maximum value near the centre of the loop. This represents the lag of the tide as it propagates through the network to converge near the centre (similar to Fig. 3). The amplitude time-series plot for PC2 varies semidiurnally and with the spring/neap tidal cycle to represent varying propagation speeds, in relation to changes in mean depth. PC3 has negative values at the western sites, positive values at the east sites and approximately a zero value near the middle. The amplitude time series for PC3 compliments the spatial variation of the shallow water tides (Fig. 4). The amplitude time series for PC3 temporally varies the same as the difference in water-surface elevation across the network, due to the tidal truncation effect. PC3 has increased magnitudes during spring tides when the truncation effect is dominant, due to increased tidal ranges. PC3 is important, as it demarcates the spatial extent of the truncation effect and delineates the slough network into three separate systems. The west side is defined by the positive values of PC3 to show the truncation effect at sites Pablo, Socr, and SNS. The component shows a lack of truncation effect on the east side defined by stations Buchli, MIC, and M5. Site Hude is located at a convergence from both sides. With these spatial variations of PC3, the study area is demarcated into three regions: west side, barotropic convergence, and east side (Fig. 8).

2.1.3. *Velocity*

The truncating sill affects the velocities by creating longer durations of slack tide at lower low water and rapid increases in velocity when the sill is overtopped. During spring tides, as the water-surface elevation reduces to the level of the sill, the influence of friction and the tidal truncating effect will reduce the magnitudes of the velocities. As seen near day 258.25 (Fig. 9b) the spring tidal water level has decreased to an elevation of 0 m MLLW at sites Pablo and SNS. At this time, the velocities have slowed to a minimal magnitude of approximately 5–10 cm s^{-1} for a duration of nearly 1.5 h at sites Pablo and SNS. At this time, tidal current at Sonoma Creek (site Socr) was ebbing slightly (not shown) from upstream wetland drainage. Current at site Pablo is limited by the sill, so the ebb must flow east past site SNS. The velocity at site SNS shows an eastward (positive) direction with a magnitude of approximately 10 cm s^{-1} towards site Hude.

The long duration of slack is ended when the rising water level in the bay overtops the sill (day 258.3),

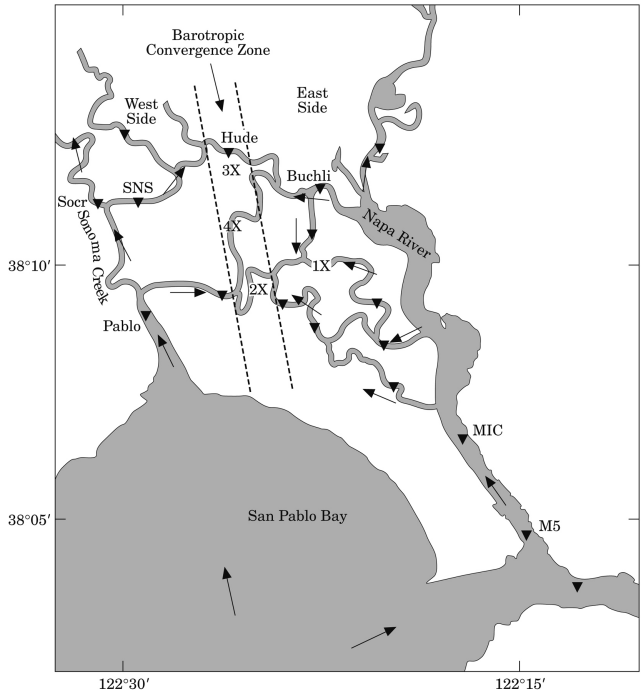

Fig. 8. Identification of slough network as three systems: west side, east side, and barotropic convergence zone in the middle. Legend: ⟶, directions of flooding current; X, location of converging currents; ▼, locations of equipment.

correlating with the sudden turn of velocities to the flood direction for sites Pablo and SNS. The velocities increase from slack to near 70 cm s^{-1} in 80 min, which is in the order of $\partial u/\partial t \sim 1 \times 10^{-4}$ m s^2, suggesting that temporal acceleration may be important. A momentum balance on the well-mixed longitudinal flow in the slough channels can be performed with the one-dimensional shallow water momentum and continuity equations described by Ippen (1966). Using the velocity and water-level field data from sites Pablo and Socr, the distance of 6100 m, and a Manning n value of 0.015, the momentum balance (in units of m s^{-2}) scales as

$$\underset{\substack{10^{-4}\\ \text{temporal}\\ \text{acceleration}}}{\frac{\partial\langle u\rangle}{\partial t}} + \underset{\substack{10^{-5}\\ \text{convective}\\ \text{acceleration}}}{\langle u\rangle\frac{\partial\langle u\rangle}{\partial x}} = \underset{\substack{10^{-4}\\ \text{barotropic}\\ \text{gradient}}}{-g\frac{\partial\eta}{\partial x}} - \underset{\substack{10^{-4}\\ \text{friction}}}{\frac{gn^2\langle u\rangle|\langle u\rangle|}{(h+\eta)^{4/3}}} \quad (1)$$

where $\langle u(x,t)\rangle$ is the cross sectionally averaged velocity, t the time, x the longitudinal direction, $\eta(x,t)$ the water-surface displacement measured positive upwards from the mean water level, and g is the acceleration due to gravity. This scaling shows that the temporal acceleration term is in the same order of magnitude as the barotropic gradient and the friction terms. Friedrichs, Lynch, and Aubrey (1992, Chap. 15) demonstrated the importance of frictionally dominated systems with minimal inertia. However, in the present system, the temporal

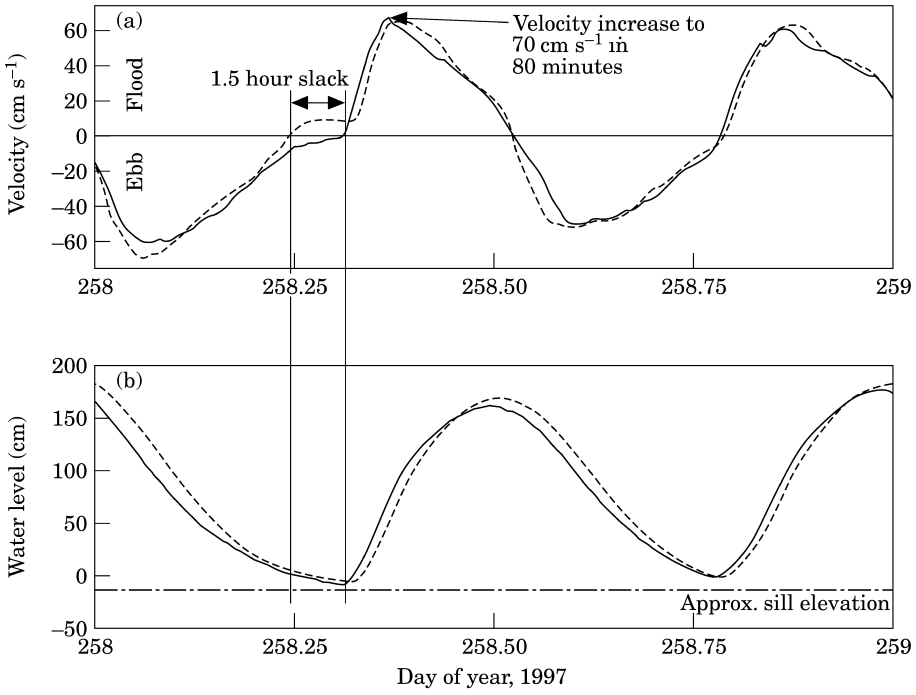

Fig. 9. Typical time series of velocity (a) and water level (b) at the western sites Pablo and SNS during a spring tide. The velocity exhibits a long period of slack while the water level cannot decrease below the sill elevation. Propagation speed of flood wave is shown on the water-level plot (—, Pablo; - - - -, SNS).

acceleration term is as important as the frictional term. The convective acceleration term is an order of magnitude less than the other terms, which is typical infrictionally dominated shallow water channels (Speer & Aubrey, 1985). At dynamic equilibrium, the acceleration is in balance with the barotropic gradient and the friction term.

A similar scaling for continuity leads to

$$\underset{\substack{10^{-4}\\ \text{temporal}}}{\frac{\partial \eta}{\partial t}} + \underset{\substack{10^{-4}\\ \text{mean depth}}}{h\frac{\partial \langle u \rangle}{\partial x}} + \underset{\substack{10^{-5}\\ \text{nonlinear}}}{\frac{\partial (\langle u \rangle \eta)}{\partial x}} = 0 \qquad (2)$$

This scaling reveals that the temporal change in the water level primarily is in balance with the spatial rate of change of the velocity times the mean depth. The nonlinear term is an order of magnitude smaller, but it affects the balance by altering the phase speed of the wave. Because η is in the order of the depth ($\eta/h \sim 0.3$), and the wave speed is a function of the depth, the wave will travel faster at high tides and slower at low tides. This effect will produce an M4 oscillation from the main tidal constituent (M2).

The velocity at site Pablo during spring tides is in phase with the discharge from the slough network but the water level is in phase with the tidal forcing from the bay. This creates high tide at site Pablo approximately 0.5 h before the end of the flood current. Thus, the ebb will have a reduced cross-sectional area, creating higher ebb velocities than normally would be observed. Similar characteristics were observed by Speer, Aubrey, and Friedrichs (1991) for a tidally truncated estuary in Pamet, MA. However, their truncation was caused by the uncoupling of the interior tide from the ocean tide by very shallow depths, creating an interior balance between bottom slope and friction, as opposed to a balance between the barotropic pressure gradient and bottom friction as was the case with the example in San Francisco Bay.

The velocity that develops during neap tides is more tidally symmetric due to the minimized influence of the sill (not shown). Duration of slack after ebb is diminished greatly.

2.2. Barotropic convergence

Tidal signals from both sides of the system meet in the convergence zone where it is more appropriate to consider the role of the water-surface (barotropic) component of the pressure gradients than the propagation of the tide. Fig. 10a shows the water-surface elevations during a spring tidal period at sites Socr (west side, showing tidal truncation) and Pipe (east side). The difference in the water-surface elevations (Fig. 10b) produces an oscillating barotropic pressure gradient across the middle convergence zone with a quarter-diurnal characteristic. The measured time series of velocity at site Hude (in the convergence zone) clearly oscillates in response to this pressure gradient (Fig. 10c). The quarter-diurnal character is greater at times of lower low water (during spring tides). For example, at day 258.25, the water-surface elevation at site Socr was greater than that at site Pipe (Fig. 10a, label 1). This difference occurred because the west side was not able to ebb fully, owing to the sill. The east side has relatively unimpeded ebb, and, therefore, the water level will decrease with the full tidal range, resulting in a higher water-surface elevation on the west side of the system driving a flow to the east. Fig. 10c shows that at this time (Fig. 10c, label 1) there is a flow to the east at site Hude.

Because the sill delays the rising tide on the west side, the east side will receive an increasing water level first and the response is to drive a flow to the west (Fig. 10c, label 2). Until the next low tide, the oscillations in the velocity are due to the differences in the rates of increase of the water levels on the west and east sides, as well as to minor influences from the network of channels.

A momentum balance (Eq. (1)) in this convergence zone is evaluated with data from site Hude (Fig. 10d) with $n = 0.015$ and by neglecting the convective acceleration term. The driving force is the barotropic pressure gradient, $g\,\partial\eta/\partial x$, estimated as the difference in water-surface elevations between sites Pipe and Socr, divided by an appropriate length scale of the length of Hudeman Slough, approximately 4.5 km. The temporal acceleration term is maximum (in the order of $10^{-4}\,\mathrm{m\,s^2}$) during times when the velocity at site Hude is changing direction from the east to the west. This is significant to show the dynamic nature of the wave. The size of the unsteady term is caused by the arrival of the wave energy, while the magnitude of the friction term is caused by the delay in water movement. The momentum balance shows a strong correlation between the sum of the temporal and friction terms and the barotropic pressure term. At moments of maximum current, a dynamic balance exists between the friction term and the barotropic gradient.

Momentum balance during neap tides is less dramatic because the tidal truncation effect is weaker. As a consequence, the water-surface elevations across the complex are then more nearly the same on the east and west sides (not shown) and the differences in water-surface elevation do not exceed 10 cm. Resulting barotropic gradients are not as strong as those occurring during spring tides. Hence weaker currents form at site Hude with maximum neap tidal currents in the order of $25\,\mathrm{cm\,s^{-1}}$. This situation contrasts with the maximum spring tidal currents that are nearly $70\,\mathrm{cm\,s^{-1}}$ (Fig. 10c).

The continuity equation can be used to explain how the quarter-diurnal velocity creates a dominant semi-diurnal water level at site Hude (not shown). During the 'flood' at site Hude, water approaches midslough

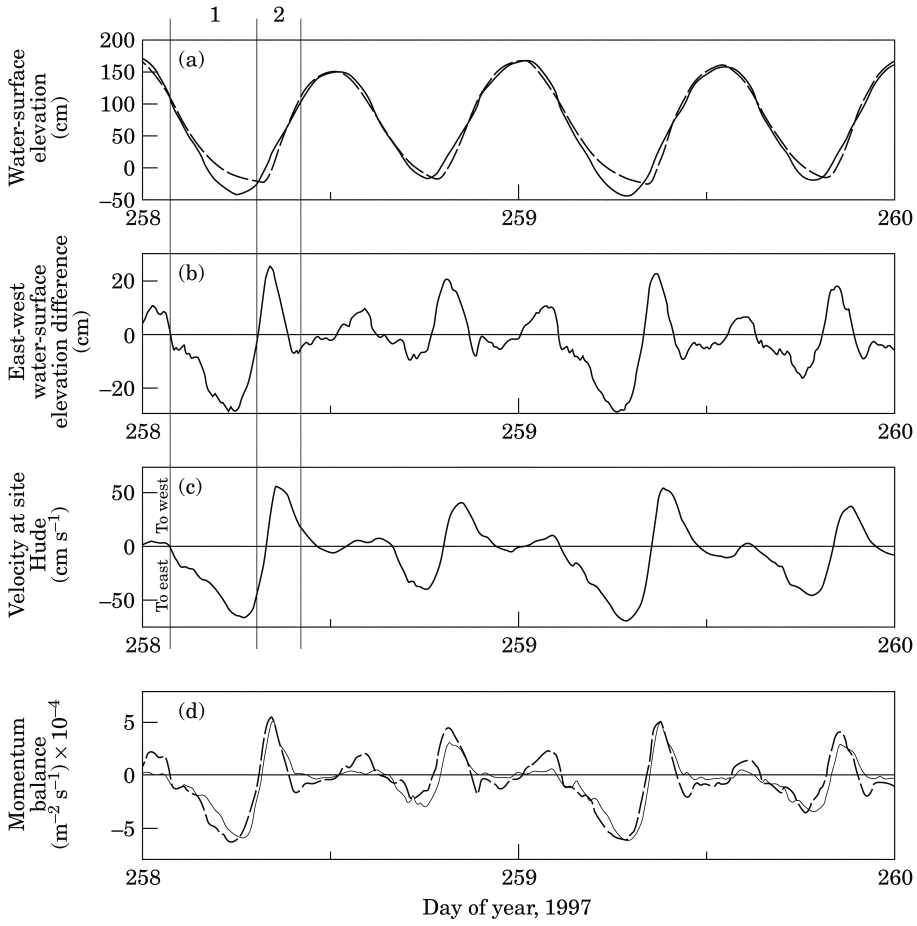

Fig. 10. Time series of water-surface elevation and velocity at the east and west sides, (a) water-surface elevations at an east site (Pipe) and west site (Socr); (b) difference in water-surface elevation between sites Pipe and Socr; (c) velocity at site Hude, positive velocity to the west, negative to the east; (d) momentum balance at site Hude. Legend (a): – – –, Socr (west side); ——, pipe (east side). Legend (d): ———, $(\partial\langle u\rangle/\partial t) + (gn^2\langle u\rangle \mid \langle u\rangle \mid /(h+\eta)^{4/3})$; – – –, $-g(d\eta/dx)$.

from both directions. Therefore, no matter which direction the velocity at site Hude is heading, it will approach as an incoming flow. Thus, there must be a location at which the velocity is zero. The velocity gradient $\partial u/\partial x$ (with x positive in the direction of flow) from site Hude to the zero velocity location always will be negative. From the continuity equation: $\partial\eta/\partial t = -h\,\partial u/\partial x$, with $\partial u/\partial x$ being negative, leads to $\partial\eta/\partial t$ being positive, implying that the water level will be increasing in time. Consequently, even though the direction of the velocity changes due to barotropic gradients during the flood, the water level only can increase. During the ebb, a similar process occurs with $\partial\eta/\partial t$ being negative. At site Hude, independent of the direction of velocity, the water level in that direction is also decreasing, which allows for the water level at site Hude also to decrease.

2.3. Water flux

The tidally averaged flux of water through the system is controlled by the residual barotropic gradients across the convergence zone. During spring tides, the tidally averaged water-surface elevation on the west side will be greater than on the east side because the sill truncates the lower water levels on the west side, thus increasing the mean water level and driving a tidally averaged flow to the east. Fig. 11 shows the water-surface elevation difference on tidal (Fig. 11a) and tidally averaged (Fig. 11b) time scales. During spring tides (day 260), the tidally averaged difference from the west to the east side is negative, indicating a higher tidally averaged water level on the west side. This higher water level allows the tidally averaged flux of water at site Hude (Fig. 11c) to move towards the east. During neap tides, the tidally averaged water level is higher on the east side of the system because the propagation speed of the tide is greater on the east side and the tidally averaged flux of water flows to the west at site Hude (near days 254 and 270).

3. Discussion

The slough network contains four convergence locations (Fig. 8), including the convergence zone located

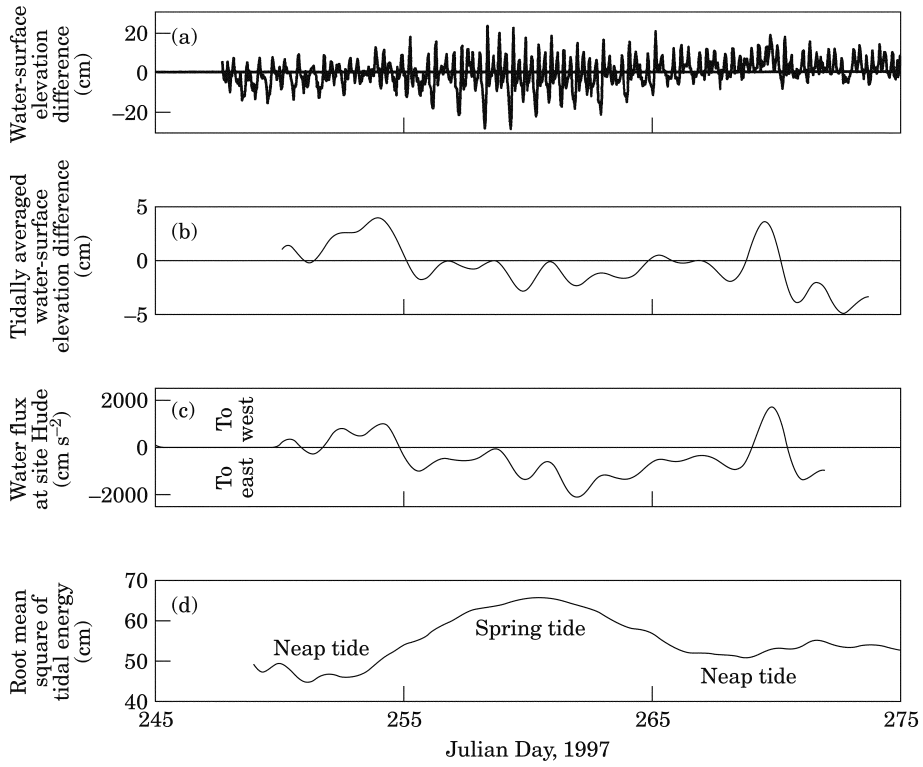

Fig. 11. Spring/neap variations of water flux past site Hude. (a) Tidal water-surface elevation difference of sites Pipe–Socr; (b) tidally averaged water-surface elevation (WSE) differences; (c) tidally averaged water flux past site Hude to the east during spring tides and to the west during neap tides; (d) measure of spring/neap tidal cycle.

near site Hude, identified by the direction and timing of measured velocities (Warner, 2000). Location '1X' is at the convergence of currents from two opposing sloughs. This location is characterized as a very narrow channel with slump blocks and vegetation in the channel. Locations '2X' and '4X' are characterized with shallow depths and very narrow vegetation-choked channels. These two locations are within one tidal excursion from San Pablo Bay, and have narrowed due to advection of sediment from San Pablo Bay, deposition of the material, and subsequent lack of shear stress on the ebb that is large enough to resuspend the material. For completeness, zone '3X' is Hudeman Slough. This slough is not subject to the same narrowing effects because large water-surface slope gradients develop along the slough, which produce barotropic gradients that keep the shear stress high enough to prevent rapid deposition.

Convergence zones are important because they can create locations where sediment and dissolved substances may accumulate. Also, these zones can act as transport pathways between two separate drainage areas. These spatial variations are consistent with observed evolutionary patterns on tidal marsh plains. For example, drainage channels can erode headwards and eventually may meet with other channels, thus creating a looped channel. The end of the looped channel that receives the rising tide first will dominate the residual flow direction and then the looped channel will act to transport material between the drainage divides on a tidally averaged time scale. On a tidal time scale, the convergence location in the loop will tend to be characterized with reduced shear stress, enhancing deposition and eventually creating a drainage divide. This divide once again separates the channels (Collins, Collins, & Leopold, 1987).

4. Summary and conclusions

Circulation patterns in a channel network driven by opposing tidal entrances are characterized by the spatial and temporal asymmetries that occur in the bounding tides. Such a channel network in San Francisco Bay is affected by a sill at the west entrance that truncates the water level during spring tides. The east side has more symmetric tidal responses. PCA was used to identify the spatial influence of the truncating sill, which led to the demarcation of the study area into three separate systems (west side, middle, and east side). Because the west and east sides produce different degrees of tidal asymmetry, the middle of the complex responds strongly to the convergence of the water levels, providing a barotropic convergence zone.

The flux of water from the west side to the east side occurs through the convergence zone and is influenced

by the spring/neap tidal cycle. Increased spring tidal ranges are truncated on the west side, producing a tidally averaged higher water-surface elevation than on the east side, which results in residual flows to the east through Hudeman Slough. During neap tides, the tidal range is reduced and flows are affected less by the sill. Tidally averaged flows then are to the west, due to faster tidal propagation along the Napa River as opposed to the shallower Sonoma Creek.

Acknowledgements

The authors acknowledge support for this research from the California Department of Fish and Game, the California Coastal Conservatory, the US Fish and Wildlife Service Coastal Program, and the US Geological Survey Federal/State Cooperative and Place-based Programs.

References

Aubrey, D. G., & Speer, P. E. (1985). A study of the non-linear propagation in shallow inlet/estuarine systems part I: observations. *Estuarine Coastal, and Shelf Science 21*, 185–205.

Collins, L. M., Collins, J. N., & Leopold, L. B. (1987). Geomorphic processes of an estuarine tidal marsh: preliminary results and hypotheses. In V. Gardner (Ed.), *International geomorphology 1986 part I* (pp. 1049–1072). New York: Wiley.

Dronkers, J. J. (1964). *Tidal computations in rivers and coastal waters* (518 pp.). New York: Interscience Publishers.

Einstein, H. A., & Fuchs, R. A. (1954). The prediction of tidal flows in canals and estuaries. First report, covering phase I of contract DA-22-079-eng-124-eng, committee on tidal hydraulics (32 pp.). Berkeley, CA. U.S. Army Corps of Engineers.

Foreman, M. G. G. (1978). Manual for tidal currents analysis and prediction. *Pacific Maine science report 78-6 Institute of Ocean Sciences,* Patricia Bay, Sidney, BC.

Friedrichs, C. T., Lynch, D. R., & Aubrey, D. G. (1992). Velocity asymmetries in frictionally-dominated tidal embayments: longitudinal and lateral variability. In D. Prandle (Ed.), *Dynamics and exchanges in estuaries and the coastal zone* (pp. 277–312). Washington, DC: American Geophysical Union.

Gartner, J. (1997). USGS Menlo Park, CA. Harmonic analysis computer program, developed by Mike Foreman. Sidney, BC, Canada: Institute of Ocean Sciences. Based on: Foreman, M. G. G. Manual for tidal heights analysis and prediction (66 pp.). Patricia Bay, Sidney, BC: Institute of Ocean Sciences. PMS report, 77-10.

Ippen, A. T. (1966). *Estuary and coastline hydrodynamics* (744 pp.). New York: McGraw-Hill.

Jaffe, B., Smith, & Zink, (1998). Sedimentation and bathymetric change in San Pablo Bay: 1856–1983 USGS, Menlo Park, CA. http://sfbay.wr.usgs.gov/access/sanpablobay/bathy/bathy.html.

Lincoln, J. M., & Fitzgerald, D. M. (1988). Tidal distortions and flood dominance at five small tidal inlets in southern Maine. *Marine Geology 82*, 133–148.

Parker, B. B. (1991). The relative importance of the various nonlinear mechanisms in a wide range of tidal interactions (review) paper 13. In B. Parker (Ed.), *Tidal hydrodynamics* (pp. 237–269). National Ocean Service, National Oceanic and Atmospheric Administration.

Parsons, W. B. (1918). The Cape Cod canal. *Transactions of the American Society of Civil Engineers 81*, 1–157. Paper 1403.

Preisendorfer, R. W. (1988). *Principal components analysis in meteorology and oceanography*. Amsterdam: Elsevier.

Speer, P. E., & Aubrey, D. G. (1985). A study of the non-linear propagation in shallow inlet/estuarine systems. Part II: theory. *Estuaries Coastal and Shelf Science 21*, 207–224.

Speer, P. E., Aubrey, D. G., & Friedrichs, C. T. (1991). Nonlinear hydrodynamics of shallow tidal inlet/bay systems. Paper 16. In B. Parker (Ed.), *Tidal hydrodynamics* (pp. 321–339). National Ocean Service, National Oceanic and Atmospheric Administration.

Walters, R. A., Cheng, R. T., & Conomos, T. J. (1985). Time scales of circulation and mixing processes of San Francisco Bay waters. *Hydrobiologia 129*, 13–36.

Warner, J. C. (2000). Barotropic and baroclinic convergence zones in tidal channels. PhD dissertation. Davis, CA: Department of Civil and Environmental Engineering, University of California.

Warner, J. C., Schladow, S. G., Schoellhamer, D. H. (1999). Summary and analysis hydrodynamics and water-quality data for the Napa/Sonoma Marsh complex. Final report, Equipment deployment from September 1997 to March 1998. Davies, CA: University of California. Environmental Dynamics Laboratory Report No. 98-07 (114 pp.).

Wilcox, B. W. (1958). Tidal movement in the Cape Cod Canal, Massachusetts. *Journal of the Hydraulics Division, Proceedings of the American Society of Engineers 1–9. Paper 1586, HY2.*

Wong, K.-C. (1990). Current and sea level variability in the Chesapeake and Delaware Canal. *Journal of Geophysical Research 95*(C10), 18343–18352.